A STUDY OF THE PERFORMANCE OF FLUSH AIR INLETS INSTALLED ON SURFACES WITH CURVATURE

Pedro Henrique Caruy Povoa, phcpovoa@gmail.com
Antonio Batista de Jesus, antonio.jesus@embraer.com.br
Embraer – Empresa Brasileria de Aeronautica S/A

Luis Fernando Figueira da Silva, luisfer@esp.puc-rio.br
Pontifícia Universidade Católica do Rio de Janeiro – PUC-Rio

Abstract. *Aircraft systems use air inlets for capturing external air flow for cooling or ventilation purposes.Flush air inlets are the most preferred type due to their low drag characteristics and better adequacy for operarion in icing conditions. Knowledge of performance curves of flush air inlets, which correspond to dynamic pressure at the inlet throat versus mass flow rate curves, is essential for correct inlet sizing guaranteeing adequate systems operation without unnecessary drag generation. Performance of flush air inlets was widely studied in the decades of 1940 and 1950 through wind tunnel testing, in which, the air inlets were normally installed on flat plates and performance curves, were determined as a function of upstream flow parameters, particularly the boundary layer momentum thickness. In real aircraft applications flush air inlets are generally not installed on flat surfaces and, to the authors' knowledge, procedures to correct inlet performance due to curvature effects are not available in the open literature. In this work, the performance of a flush air inlet installed on a curved surface is studied using computational fluid dynamics. After validation of a mesh generation strategy, three-dimensional models of a flush air inlet with NACA divergent ramp profile installed on three different positions on a bump were generated. Inlet performance is determined as a function of inlet air mass flow rate for a Mach number and the results are compared to those obtained for the installation of the same inlet on a flat plate. It is observed that the total pressure profiles upstream of the inlet ramp plays a major role on the inlet performance curve and that an a priori estimate of inlet performance can be obtained from the average total pressure along a distance equivalent to the inlet throat height.*

Keywords*: NACA Inlet, Air Inlet, Ram Recovery Ratio, CFD, Performance*

1. INTRODUCTION

Flush air inlets are widely used in commercial and business jets in order to provide cooling and/or ventilation air for systems and compartments. Typical applications include cooling for the air-conditioning systems and electrical generators as well as ventilation of compartments subject to flammable fluid leakage. Due to their low drag characteristics, flush air inlets are preferred to more protruding scoop-type inlets, although scoop inlets tend to have better performance. Icing environments operation is also more favorable for flush inlets, when compared to protruding scoops.

Performance of flush air inlets was widely studied in the 1940 and 1950 decades by means of wind tunnel measurements. The widely-known outcame of those investigations is the so-called NACA divergent ramp flush air inlet, also dubbed the NACA inlets, which can be found in virtually every commercial aircraft currently in operation.

In those wind-tunnel tests, the air inlets were usually installed on flat plates and performance curves, which correspond to dynamic pressure at the throat inlet as function of mass flow rate curves, were determined for a range of freestream flow parameters, particularly the boundary layer momentum thickness. The ESDU86002 (2004) document is a compilation which provides parametric performance data of flush air inlet based on such experimental results.

More recently, Perez et al. (2007) used CFD to determine the performance of NACA flush air inlets installed on flat plates and the effects of installing vortex generators upstream of the inlet. The presented results allow to verifying a good agreement between the performance curves of flush air inlets calculated by CFD and that obtained from the parametric curves of ESDU86002.

In aircraft applications flush air inlets are, generally, not installed on flat surfaces. Although some wind tunnel investigations were performed with flush air inlets mounted on surfaces with curvature, as in the work of Hall and Barclay (1948), to the authors' knowledge procedures to account for curvature effects on flush air inlets performance are not available in the open literature. A more comprehensive review of the state of the art of flush air inlets may be found in Perez et al. (2007).

In this work, the performance of NACA air inlets installed on a curved surface is studied using computational fluid dynamics (CFD). First, a new mesh generation scheme based on tetrahedrals and a prism layer is validated for the calculation of flush air inlets performance by comparison with the results of Perez et al. (2007), which used hexahedral meshes. The aim is to develop a more flexible meshing when compared to previous works, thus allowing for easier geometrical configuration modifications. A second step consisted in using the tetra/prism mesh methodology to study the installation effects of a NACA air inlet on different locations on a curved surface. The third step consists on evaluation of the performance of flush air inlets for three different locations along the curved surface.

Calculated mass-flux average total pressure at the inlet throat along with the imposed mass-flow rate value were used to obtain inlet ram-recovery ratio and mass-flow ratio, which are defined as

$$\eta_{fl} = \frac{p_{t_{TH}} - p_0}{p_{t_o} - p_0} \tag{1}$$

$$MFR = \frac{\rho V A_{th}}{\rho_\infty V_\infty A_{th}} \tag{2}$$

where $p_{t_{th}}$, is the inlet throat total pressure; p_0, is the freestream static pressure; p_{t_0}, is the freestream total pressure; ρ, is the inlet density; ρ_∞, is the freestream density; V, is the inlet average velocity; V_∞, is the freestream velocity and A_{th}; is the throat area.

Finally, a method to perform a preliminary assessment of curvature effects on the performance of a flush air inlet is proposed.

2. NUMERICAL METHODOLOGY

Numerical simulations were performed in order to solve the three-dimensional continuity, momentum and energy equations for the flow of air, considered an ideal gas, in the domains of interest. Turbulence is modeled using a two-equation realizable k-epsilon turbulence model for the Reynolds-averaged Navier-Stokes equations. Walls are assumed adiabatic and wall functions are used for treating viscous effects.

The commercial CFD package from Metacomp Technologies, CFD++, version 7.1.1, is used for all simulations. According to Peroomian et al. (1997), in CFD++ “the numerical solution of the Reynolds-averaged Navier-Stokes equations is based on an integral form of the conservation laws that is discretized in space using a new second order multidimensional vertex-oriented TVD (Total Variation Diminishing) scheme coupled with suitable pointwise implicit or explicit time integration”. In addition, “the finite volume framework adopts for the integral conservation laws updates of cell averages in time insuring correct signal propagation via a modified Roe’s Riemann solver”. A preconditioned form of the equations is used which is more suitable for low-speed (Mach 0.3) conditions considered in this study.

More details about the CFD++ code structure may be found in the works of Chakravarthy et al. (2000), Jesus et al. (2002), Jesus et al. (2004) and Metacomp Technologies homepage in http://www.metacomptech.com/.

3. RESULTS AND DISCUSSION

This section presents, firstly, a comparison between the results obtained with different mesh generation strategies, then, a parametric study of the inlet performance for different positions along a curved surface. For each section are presented the geometrical configuration and the corresponding mesh and boundary conditions.

3.1. Influence of Mesh Type: Hexahedral vs. Tetra-Prism Meshes

In this section, a flat plate installed NACA inlet is analyzed with the use of two different types of meshes: a hexahedral mesh and a tetrahedral mesh with a prism layer over the flat plate where the inlet was installed. The geometrical configuration and the hexahedral mesh are identical to those studied by Perez et al. (2007).

The 10.4 º ramp angle NACA inlet was placed at the center of a 10 m x 2 m flat plate positioned at a distance of 5 m downstream to the beginning of the flat plate. In order to simulate actual operating conditions, an exit duct of 120 mm x 30 mm rectangular cross section and 500 mm length was coupled to the NACA inlet throat. Since the assembly NACA inlet, flat plate, and exit duct are symmetrical with respect to the centerline of the NACA inlet, a half model was used. Thus, as can partly be seen in Fig. 1, the computational domain consisted of a box of 10 m x 1 m x 1 m.

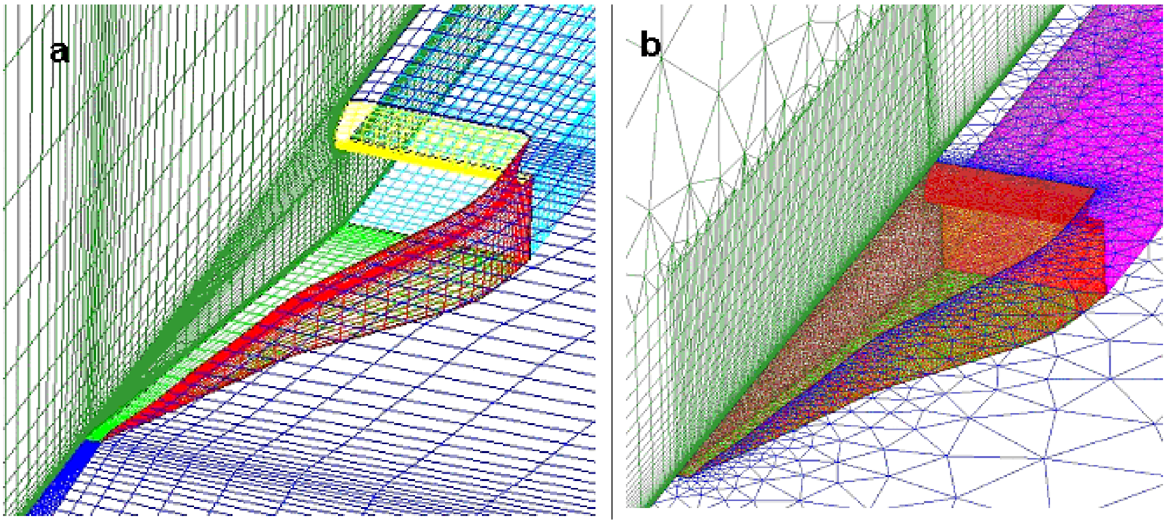

Figure 1. Hexahedral and tetrahedral mesh with prism layer.

The grid generation of the studied configuration was performed using the software ANSYS ICEM CFD version 11.1. The hexahedral structure mesh generated consisted of 226000 hexahedral elements, refined mostly at the boundary layer region of the flat plate and inside the inlet and duct, as shown in Fig. 1a.

The tetra-prism mesh consists of 1.2e6 tetrahedral volumes placed inside the inlet, exit duct and above the prism layer which included 400000 prism elements normal to the flat plate and above an inlet cover. This cover allowed to build a constant height prism layer over the region above the flat plate, thus adequately representing the inlet upstream boundary layer. The prism layer has a total height of 80 mm split in 38 layers, with a first layer height of 0.06 mm and a growth ratio of 1.2. Figure 1 shows a close up view of both meshes at the vicinity of the air inlet.

In this analysis, computational domain “far field” boundary is where freestream flow conditions, i.e. a Mach number of 0.3, a temperature of 270.32 K and a static pressure of 72428 Pa are specified. These values are equivalent to a 9000 ft flight condition. At the duct exit section, a uniform static pressure was adjusted during simulations in order to reach a specified mass-flow rate target. No-slip adiabatic boundary conditions were set at all the solid walls and symmetry condition was specified at the symmetry plane of both meshes.

Simulations were performed for a range of mass-flow rates imposed at the inlet duct. Convergence was verified by monitoring residuals drop by four orders of magnitude and stabilization of mass-flow rate and mass flux average total pressure at the inlet throat.

Figure 2 shows calculated performance curves for both meshes along with results obtained from the parametric curves of ESDU86002. A good agreement can be observed between both CFD results and the ESDU data, with differences lower than 10%. The hexahedral mesh and tetra-prisms mesh results were found to disagree less than 1%.

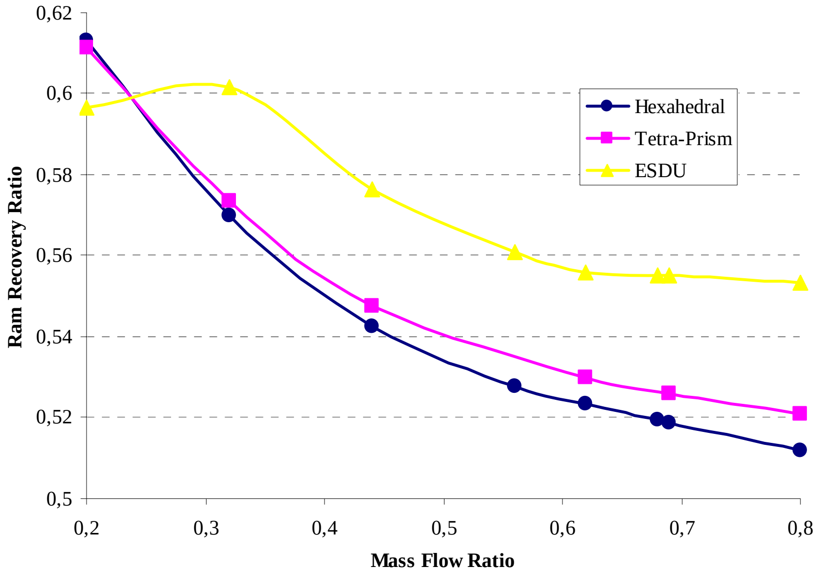

Figure 2. Characteristic curve of ram-recovery ratio of the conventional Naca inlet.

These results allow to conclude that the tetra-prisms mesh proposed can be used for the determination of NACA inlets performance. Such a simpler mesh generation scheme will be employed for the subsequent computations where a NACA inlet installed in different positions on a surface with curvature is studied.

3.2. NACA Inlet Installed in a Curved Surface

Computations were performed considering a NACA inlet installed on a curved surface (bump) inside a wind tunnel. The bump surface has a maximum height above the tunnel floor of 200 mm, a radius of 1.7 m, and its center is located exactly at the center of the tunnel (4 m long, 1.3 m x 1 m cross section). A transition curve at its trailing edge exists in order to smooth curvature change. Figure 3 shows more details of the geometry analyzed.

The studied NACA inlet has a ramp angle of 7º with a 10 mm throat height and 40 mm throat width. The lip is elliptical with a 5 mm thickness and the 106.5 mm length exit duct, was curved for installation purposes. Figure 4 shows more details of the inlet geometry.

The inlet was installed in three different positions along on the bump in order to be submitted to different flow conditions, in terms of local static pressure, pressure gradient and boundary layer thickness. Calculations were also performed for the same NACA inlet installed on a flat plate inside the same wind tunnel and in the absence of the bump. The inlet was located in positions at the beginning and the end of the bump.

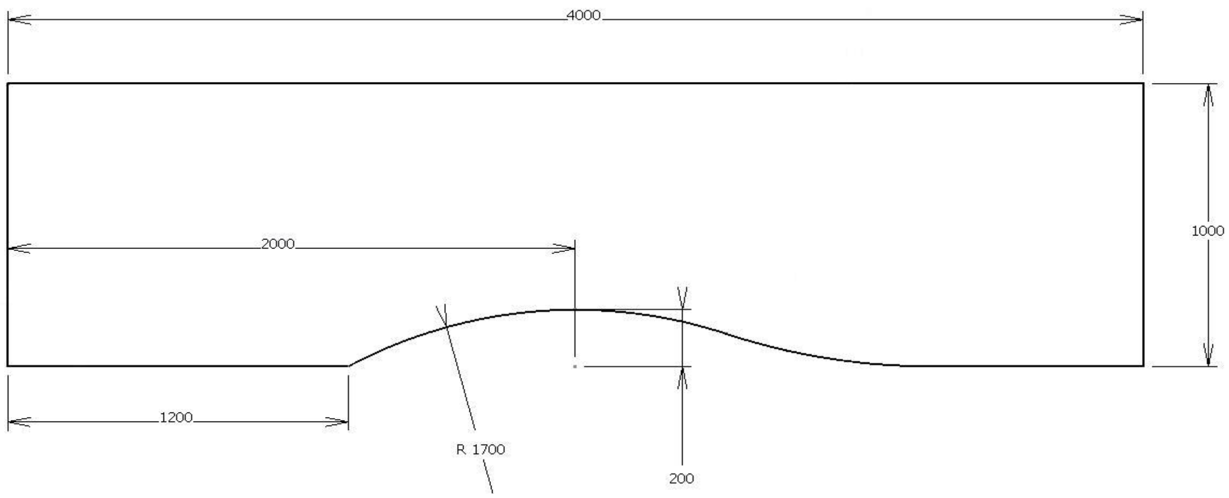

Figure 3. Lateral view of the wind tunnel geometry.

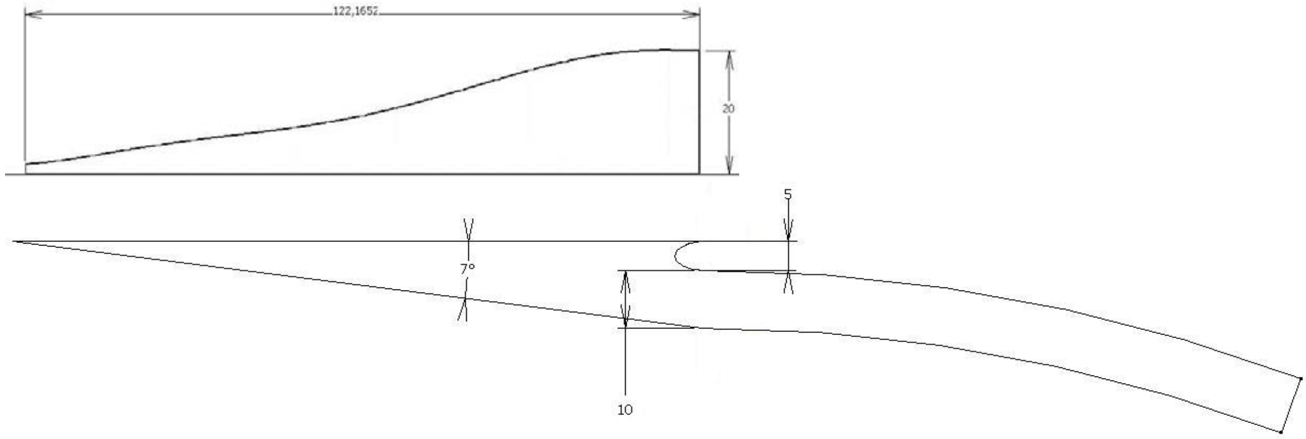

Figure 4. Top and lateral view of the Naca inlet.

Grid generation was performed using the ANSYS ICEM CFD software with tetrahedral elements and a prism layer over the surface of the tunnel floor. The grid had 486000 tetrahedral volumes placed inside the inlet entrance, exit duct and above the prism layer which consisted of a 262000 prism elements grown normal to the wind-tunnel floor and the bump. The prism layer has 80 mm of total height split in 38 layers, with a height of 0.06 mm for the first layer and a growth ratio of 1.2. Figure 5 shows overall and close-up views of the surface mesh at the symmetry plane and inlet.

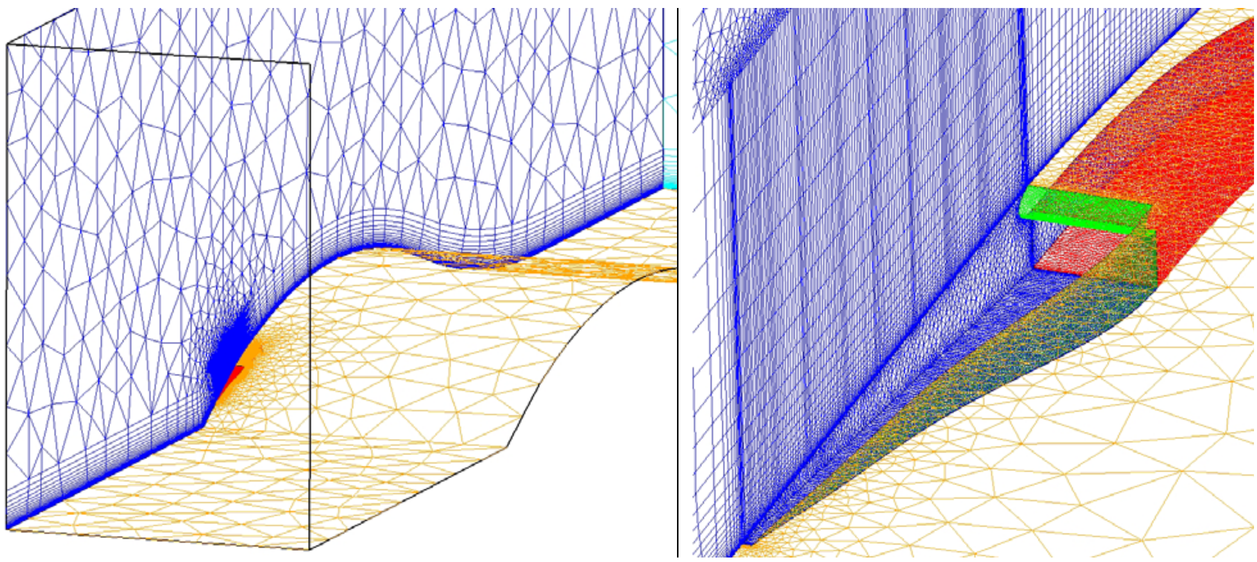

Figure 5. Surface mesh at the symmetry plane and inlet.

Freestream conditions are identical to the previous case, i.e. Mach 0.3, static temperature of 270.32 K and static pressure of 72428 Pa. At the duct exit section, a uniform static pressure is adjusted, during simulations, in order to obtain a specified mass-flow rate.

Simulations were again performed for a range of mass-flow rates imposed at the duct. Convergence by four orders of magnitude is also verified by monitoring stabilization of mass-flow rate and mass flux average total pressure at the inlet throat. Note that, for some of the low mass-flow ratio conditions it was not possible to obtain a converged solution and, thus, those results are not reported.

Prior to the definition of the NACA inlet locations on the bump, a simulation of the bump without air inlets is performed in order to determinate positions where the inlet could be submitted to positive and negative pressure coefficients and also favorable and adverse pressure gradients. Figure 6 shows the pressure coefficient on the bump without the inlets. The lines drawn in Figure 6 are normal to the bump at the location chosen for the beginning of the inlet ramps. Thus, the NACA inlets are then installed in the front, middle and rear of the curved surface.

An a priori estimate of the effectiveness of positioning the NACA inlet may be attempted by comparing the total pressure evolution along the lines shown in Fig. 6 to that obtained for a flat plate. Figure 7, that presents such a comparison, shows that, as could be expected, the total pressure deficit increase with the distance along the flat plate. Furthermore, the presence of the bump substantially influences the total pressure evolution along the plate normal.

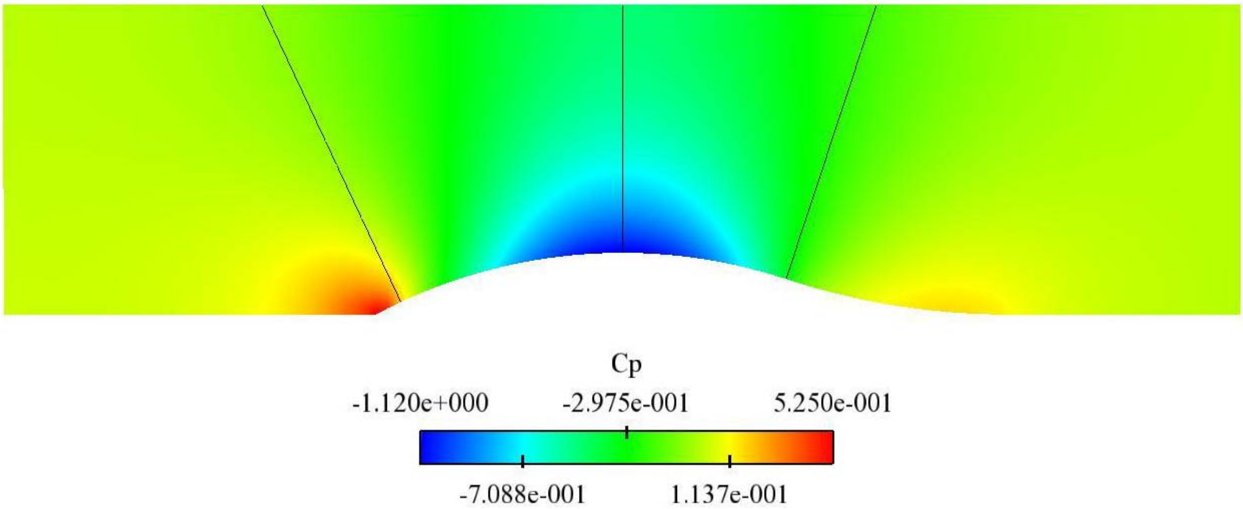

Figure 6. Pressure coefficient around the bump surface without air inlets.

Indeed, the total pressure is much smaller at the downstream positions than at the upstream, windward side. Since direct connection exists between the total pressure and the boundary layer momentum thickness, which in turn influences the inlet performance, a measure of expected inlet efficiency could be could be achieved by the integral of the total pressure normal at the surface. Furthermore, using as integration length scale, the inlet throat height, one can obtain an average total pressure which would correspond to the maximum achievable efficiency if the inlet throat could be aligned with the local streamlines. Such an efficiency is plotted in Fig. 8 together with the computed performance curves for the NACA air inlet installed on different bump locations and at a flat surface in stations corresponding to the beginning and end of the bump.

From Fig. 8 it can be observed that for the inlet placement on the bump underperforms the corresponding flat plate results at the middle and the end of the bump positions.

The inlet performance is strikingly low when placed at the bump leeward side, exhibiting a ram-recovery ratio of less than 5%. A performance increase is observed when the inlet is positioned at the bump windward side only.

From Figure 8 it can also be noticed that the external ram-recovery ratio integration can be used to provide a reference value for the maximum ram-recovery ratio available at the inlet throat. These results show that the order of magnitude of the differences between the calculated performances for different inlet locations, shown in Fig. 8, could be predicted by using this technique.

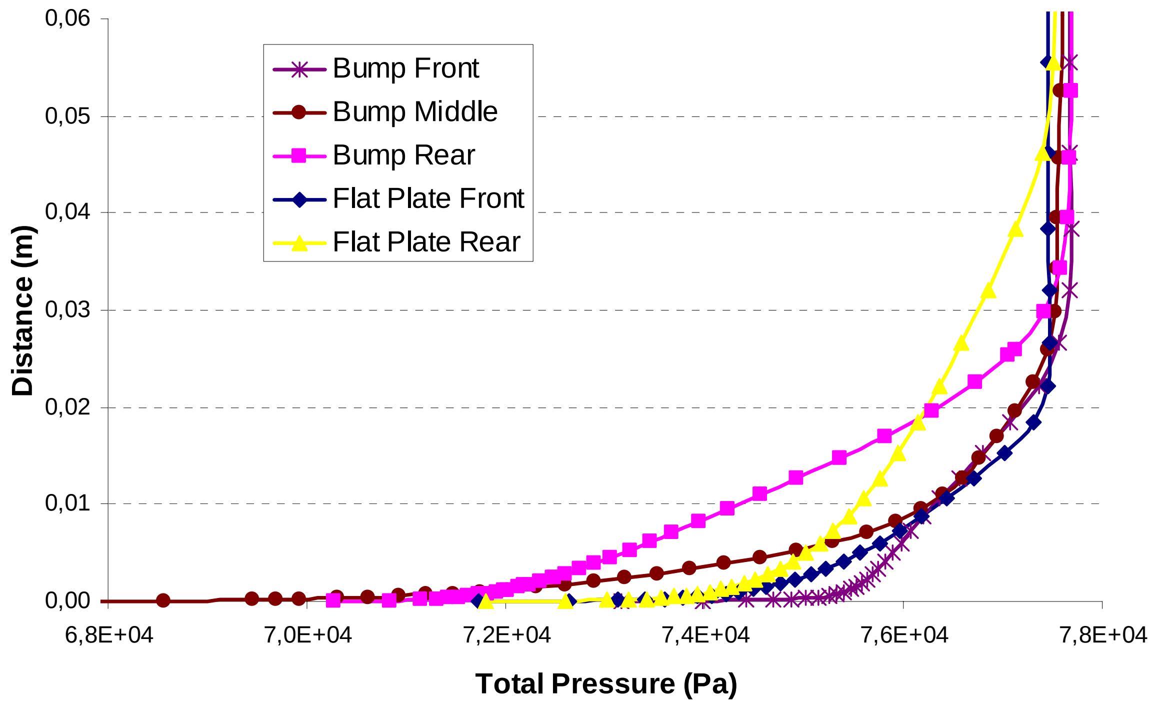

Figure 7. Total pressure boundary layer at the beginning of the inlet ramp

It is worth noting, though, that for high values of the mass flow ratio, the actual computed inlet performance is smaller than the one predicted by integration of the total pressure evolution. This difference could be related to inlet flow distortion, characteristic of NACA inlets, or to inefficiencies inherent to submerged inlets. A comparison between NACA and parallel ramp inlets, out of the scope of this paper, could shed some light on this matter.

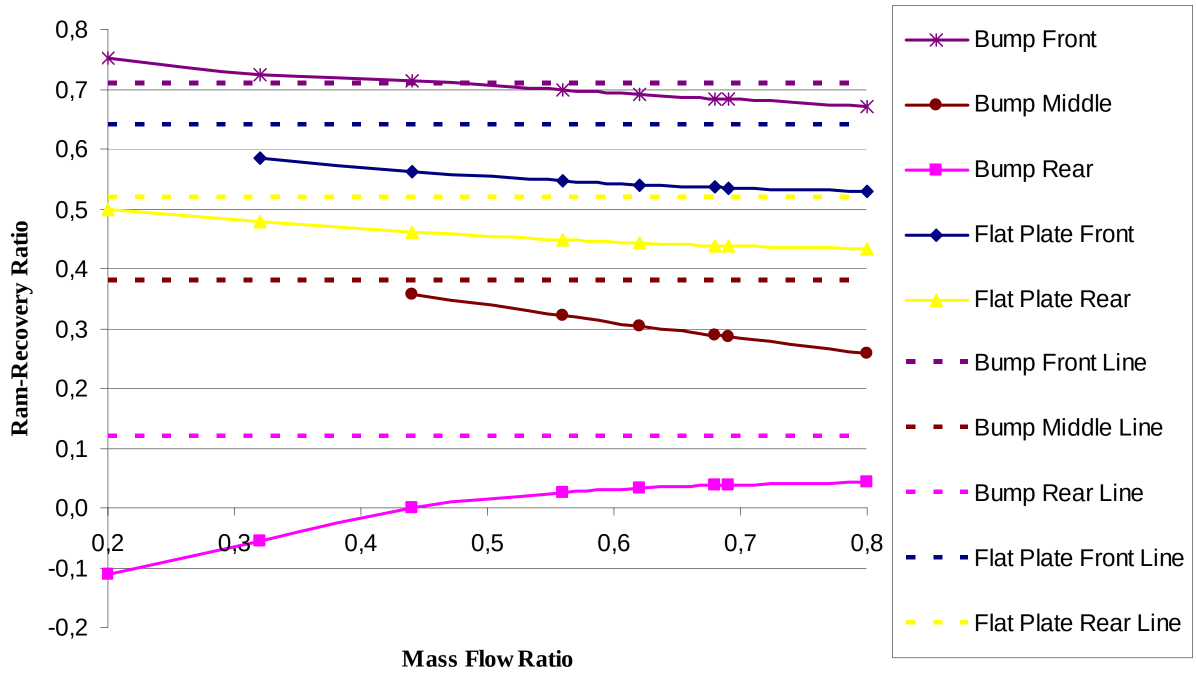

Figure 8. Ram-recovery efficiencies of the Naca inlets installed in a curved surface and in a flat plate and the maximum ram-recovery ratio available at the inlet.

5. CONCLUSIONS

This paper presented a study of the performance of flush air inlets installed on surfaces with curvature using CFD. The use of a more flexible tetrahedral with prism layer mesh generation scheme for calculation of NACA air inlets performance was successfully validated by comparison to the results from hexahedral meshes of Perez et al. (2007) and with those obtained from the parametric curves of ESDU86002

The performance of a NACA air inlet installed on three different locations along a bump and along a flat plate was computed. The differences between the computed performance curves could be explained by analyzing the total pressure immediately upstream to the proposed inlet location. An external ram recovery ratio was computed as a function of the average total pressure in a direction normal to the surface and up to a distance equivalent of the NACA inlet throat thickness. It was verified that the external ram recovery could be indeed a reference value, based on external flow parameters only, for the maximum achievable inlet recovery at the inlet throat.

As seen on the simulations, the best position for installing a NACA inlet is in front of the bump, followed respectively by the flat plate installations, the middle and the end position of the bump. This latter position is the most representative of the NACA inlet installation on aircraft applications, since most airplane air inlets are located where thick boundary layer and adverse pressure gradient occur. Therefore, this study underscores the need of using devices, such as vortex generators, for increasing the maximum efficiency of airplane air inlets.

In this work, calculations were performed for specific geometries (NACA inlet and bump), a single freestream condition (Reynolds and Mach numbers), using a single mesh refinement and a 2-equation realizable k-epsilon turbulence model. Thus, future works should explore different geometrical and freestream parameters, along with mesh refinement and turbulence modeling. The ultimate objective would be the capability of reasonably estimating the performance of flush air inlets installed on real aircraft as a function of external flow parameters, as the external ram recovery ratio defined herein.

6. REFERENCES

"Drag and Pressure Recovery Characteristics of Auxiliary Air Inlets at Subsonic Speeds", Engineering Sciences Data Unit, Rept. 86002 with Amendment D, London, 2004.

Perez, C. C., Ferreira, S. B., Figueira da Silva, L. F., Jesus, A. B. and Oliveira, G. L., "Computational Study of Submerged Air Inlets Performance Improvement Using Vortex Generator", Journal of Aircraft, Vol. 44, No. 5, pp. 1574-1587.

Hall, C. F., Barclay, D. F., "An Experimental Investigation of NACA Submerged Inlets at High Subsonic Speeds, I – Inlets Forward of the Wing Leading Edge", Research Memorandum, National Advisory Committee for Aeronautics, Ames Aeronautical Laboratory, 1948, Moffet Field, California

Peroomian O., Chakravarthy, S., Goldberg, U., 1997, "A 'Grid Transparent' Methodology for CFD", AIAA paper No. 97-0724, AIAA Aerospace Sciences Conference, Reno, USA.

Chakravarthy, S., Bose, T., Batten, P., Palaniswamy, S., Goldberg, U. and Peroomian, O., 2000, "Convective Heat Transfer Inside Rotating Tubes", AIAA Paper No. 00-3356, 36th AIAA/ASME/SAE/ASEE Joint Propulsion Conference and Exhibit, Huntsville, Alabama, USA.

Jesus, A. B., Damian, R. B., Oliveira, G. L., 2002, "Estudo Comparativo de Códigos Comerciais de CFD na Solução de Problemas Simples de Escoamentos Compressíveis e Incompressíveis", Proceedings of the 09th Braziliam Congress of Thermal Engineering and Sciences, Caxambu-MG, Brazil.

Jesus, A. B., Takase, V. L., Vinagre, H. T. M., 2004, "CFD Evaluation of the Discharge Coefficient of Outlets in the Presence of an External Flow", Proceedings of the 10th Braziliam Congress of Thermal Engineering and Sciences, Rio de Janeiro-RJ, Brazil.

7. ACKNOWLEDGMENTS

This work was performed while the third author was a visiting researcher with a scholarship from ANP (Agência Nacional do Petróleo, Gás Natural e Biocombustíveis), on leave from Centre National de la Recherche Scientifique (CNRS, France).